Original Article

Information Conveyed by Neuron Populations

Firing rate, Fluctuation and Synchrony

Hideo Hasegawa

Abstract

Recent neuronal experiments have shown that a population of firing neurons may carry not only mean firing rate but also fluctuation and synchrony. In order to theoretically examine this possibility, we have investigated responses of neuronal ensembles to three kinds of inputs: mean, fluctuation and synchrony driven inputs. Equations of motion for mean firing rate, fluctuation and synchrony in neuron ensembles described by the rate-code model, are derived with the use of the augmented moment method which was previously proposed for a study of stochastic ensembles with finite populations. Results calculated by the augmented moment method are in good agreement with those by direct simulations. It has been shown by the independent component analysis of our results that information on mean firing rate, fluctuation and synchrony may be independently conveyed in neuron populations. The calculated input-output relation of mean firing rates is shown to have higher sensitivity for larger multiplicative noise, as recently observed in prefrontal cortex.

Key Words: neuron ensemble, population rate code, firing rate, fluctuation, synchrony

NeuroQuantology 2008; 2:105-118

1. Introduction

There has been a long-standing controversy whether information in brain is carried by firing rate (*rate-code hypothesis*) or by firing timing (*temporal-code hypothesis*) (Rieke et al., 1996; Ursey and Reid, 1999; de Charmes and Zador 2000). Some neuronal experiments have supported the former while others the latter. A recent success in brain-machine interface (BMI) (Chapin et al., 1999; Anderson et al., 2004), however, strongly suggests that the population rate code is employed in sensory and motor neurons, though it is still controversial which of rate, temporal or other codes is adopted in higher-level cortical neurons.

Abbreviations list
AMM: augmented moment method
DS: direct simulation
FPE: Fokker-Plank equation
HH: Hodgkin-Huxley
ICA: independent component analysis
IF: integrate-and-fire
ISI: interspike interval

In recent years, much attention has been paid to a study on effects of mean firing rate, its fluctuation and synchrony (or spatial correlation) (for a review on rate and synchrony, see Salinas and Sejnowski, 2001). The precise role of synchrony in information transmission and the relation among the firing rate, fluctuation and synchrony are not clear at the moment (Riehle et al, 1997; de

Corresponding author: Hideo Hasegawa
Address: Professor of Department of Physics, Tokyo Gakugei University, 4-1-1 Koganei, Tokyo 184-8501, Japan
Phone: +81-42-329-7482 and Fax: +81-42-329-7482
E-mail: hideohasegawa@goo.jp

Oliveira et al., 1997; Tiesinga et al., 2000; Fries et al., 2001; Salinas and Sejnowski, 2001; Chance et al., 2002; Reyes 2003; Grammont and Riehle, 2003; Tiensinga and Sejnowski, 2004; Silbergberg et al., 2004; Ariero et al., 2007). The firing rate and synchrony are reported to be simultaneously modulated by different signals. For example, in motor tasks of monkey, firing rate and synchrony are considered to encode behavioral events and cognitive events, respectively (Riehle et al, 1997). During visual tasks, rate and synchrony are suggested to encode task-related signals and expectation, respectively (de Oliveira et al., 1997). A change in synchrony may amplify behaviorally relevant signals in V4 of monkey (Fries et al., 2001). An increase in synchrony of input signals is expected to yield an increase in output firing rate. The synchrony of neurons in extrastriate visual cortex is, however, reported to be modulated by selective attention even when there is only small change in firing rate (Tiensinga and Sejnowski, 2004). Rate-independent modulations in synchrony are linked to expectation, attention and livalry (Salinas and Sejnowski, 2001). Fluctuations of input signals have been reported to modify the f-*I* relation between an applied dc current *I* and autonomous firing frequency f although its sensitivity to input fluctuation seems to depend on a kind of neurons (Chance et al., 2002; Silbergberg et al., 2004; Ariero et al., 2007). The f-*I* curve of prefrontal cortex retains the increased sensitivity to input fluctuations at large *I*, while that of somatosensory cortex (SSC) is insensitive to input fluctuation though its linearity is increased at small *I* (Ariero et al., 2007).

Theoretical studies on neurons have employed two types of models. In the temporal-code hypothesis, the firing mechanism of neurons is described by conductance based models such as Hodgkin-Huxley (HH), FitzHugh-Nagumo and integrate-and-fire (IF) models, whose dynamics determines firing times of the neuron. In contrast, in the rate-code hypothesis, neurons are regarded as a black box receiving and emitting signals expressed by the firing rate. The typical rate-code models are the Hopfield model (Hopfield, 1982) and Wilson-Cowan model (Wilson and Cowan, 1972). The problem on firing rate, fluctuation and synchrony discussed above has been extensively studied by simulations with the use of spiking neuron models (Tranb et al., 1996; Wang and Buzsaki, 1996; Tiesinga et al., 2000; Golomb and Hansel, 2000; Hansel and Mato, 2003; Tiesinga and Sejnowski, 2004; for a review on calculations using IF model, see Burkitt 2006a; 2006b).

It is the purpose of the present paper to examine the same problem by using the rate-code model, which is an alternative theoretical model to the spiking model. We have investigated responses of neuron ensembles described by the rate-code model, to three kinds of inputs: mean rate-driven, fluctuation-driven and synchrony-driven inputs. Calculations have been performed with the use of direct simulations (DSs) and the augmented moment method (AMM) which was developed for a study of stochastic systems with finite neuron populations (Hasegawa, 2003a; 2006). In the AMM, we pay our attention to global properties of neuronal ensembles, taking account of mean, and fluctuations of local and global variables. The AMM has the same purpose to effectively study the properties of neuronal ensembles as approaches based on the population-code hypothesis (Rodriguez and Tuckwell, 1996; Knight, 2000; Omurtag et al. 2000; Eggert and Hemmen, 2000). The AMM has been nicely applied to various subjects of neuronal ensembles (Hasegawa, 2003b) and complex networks (Hasegawa, 2004; 2005). With the use of the AMM, we will derive equations of motion for mean firing rate, fluctuation and synchrony, in order to investigate the response to mean-fluctuation- and synchrony-driven inputs. This study clarifies, to some extent, their respective roles in information transmission.

2. Results

Rate-code model

We have adopted the rate-code model for an N-unit neuron ensemble, in which dynamics of the firing rate $r_i(t)$ (≥ 0) of a neuron *i* is given by (Hasegawa, 2007a; 2007b)

$$\frac{dr_i}{dt} = -\lambda r_i + H(u_i) + \alpha r_i \eta_i(t) + \beta \xi_i(t),$$

(for $i = 1$ to N) **(1)**

with

$$u_i = (w/Z)\sum_{j(\neq i)} r_j + I_i(t), \quad \textbf{(2)}$$

$$H(u) = u/\sqrt{1+u^2}. \quad \textbf{(3)}$$

Here λ stands for the relaxation rate: w expresses the coupling strength: Z $(=N-1)$ denotes the coordination number: $I_i(t)$ is an external input whose details will be discussed below: α and β express magnitudes of multiplicative and additive noise, respectively, represented by zero-mean white noise η_i and ξ_i with unit dispersion. The gain function $H(u)$ in Eq. (3) expresses the response of a rate output (r) to a rate input (u). It has been shown that, when spike inputs with mean firing rate r_i are applied to a HH neuron, mean firing rate r_o of output signals is r_o **;** r_i for $r_i \leq 60$ [Hz], above which r_o shows the saturation behavior (Hasegawa, 2000; Wang, Wang and Liu 2006). The nonlinear, saturating behavior in $H(u)$ arises from the fact that a neuron cannot fire with the rate of $r > 1/\tau_r$ $(\equiv r_{max})$ where τ_r denotes the refractory period and r_{max} the maximum firing rate. The rate in Eq. (3) is normalized by r_m .

With the use of the diffusion-type approximation, a spatially correlated input of $I_i(t)$ in Eq. (2) is assumed to be given by

$$I_i(t) = \mu_I(t) + \delta I_i(t), \quad \textbf{(4)}$$

with

$$\langle \delta I_i(t) \rangle = 0, \quad \textbf{(5)}$$

$$\langle \delta I_i(t) \delta I_j(t') \rangle = \gamma_I(t)[\delta_{ij} + (1-\delta_{ij}) S_I(t)]\delta(t-t') \quad \textbf{(6)}$$

where variance (γ_I) and covariance ($\gamma_I S_I$) are given by

$$\gamma_I(t) = N^{-1}\sum_i \left\langle \delta I_i(t)^2 \right\rangle, \quad \textbf{(7)}$$

$$\gamma_I S_I(t) = (NZ)^{-1}\sum_i \sum_{j(\neq i)} \left\langle \delta I_i(t) \delta I_j(t) \right\rangle, \quad \textbf{(8)}$$

$S_I(t)$ expressing the measure of correlation. We will discuss responses of the neuronal ensemble described by Eqs. (1)-(3) to the spatially correlated input $I_i(t)$ given by Eqs. (4)-(6) with given $\mu_I(t)$, $\gamma_I(t)$ and $S_I(t)$ by using both DSs and the AMM (Hasegawa, 2003a; 2006).

The augmented moment method

In discussing properties of the neuronal ensembles with the AMM, we take into account mean (μ), averaged fluctuations in local (γ) and global (ρ) variables defined by

$$\mu(t) = \langle R(t) \rangle = N^{-1}\sum_i \left\langle r_i(t) \right\rangle, \quad \textbf{(9)}$$

$$\gamma(t) = N^{-1}\sum_i \left\langle [\delta r_i(t)]^2 \right\rangle, \quad \textbf{(10)}$$

$$\rho(t) = N^{-2}\sum_i \sum_j \left\langle \delta r_i(t) \delta r_j(t) \right\rangle, \\ = \left\langle [R(t) - \mu(t)]^2 \right\rangle, \quad \textbf{(11)}$$

where $\delta r_i(t) = r_i(t) - \mu(t)$, $R(t) = N^{-1}\sum_i r_i(t)$, and the bracket $\langle \cdot \rangle$ expresses the average over the distribution of $p(\{r_i\},t)$ [Eq. (46)].

It is noted that from the second-order statistics of local (γ) and global fluctuations (ρ) of firing rates, we may evaluate the synchrony of a given neuron ensemble. The synchronization is conventionally discussed for firing timings (*temporal synchronization*) or phase (*phase synchronization*). We discuss, in this paper, the synchronization for firing rate (*rate* or *frequency synchronization*). We may define the normalized ratio for the synchrony of firing rates in terms of $\gamma(t)$ and $\rho(t)$, as given by (Hasegawa, 2003a; see Eq. (51) in Materials and Methods)

$$S(t) = (N/Z)[\rho(t)/\gamma(t) - 1/N], \quad \textbf{(12)}$$

which is 0 and 1 for complete asynchronous and synchronous states, respectively.

After some manipulations, we get equations of motion for $\mu(t)$, $\gamma(t)$ and $S(t)$ given by (see Eqs. (47)-(49) in Materials and Methods)

$$\frac{d\mu}{dt} = -\lambda\mu + h_0 + \alpha^2\mu/2, \quad \textbf{(13)}$$

$$\frac{d\gamma}{dt} = -2\lambda\gamma + 2h_1 w\gamma S + 2\alpha^2\gamma + \gamma_I + \alpha^2\mu^2 + \beta^2, \quad \textbf{(14)}$$

$$\frac{dS}{dt} = -\frac{(\gamma_I + \alpha^2\mu^2 + \beta^2)}{\gamma} S + (\gamma_I S_I / \gamma) + (2h_1 w / Z)(1 + ZS)(1 - S). \quad \textbf{(15)}$$

In Eqs. (13)-(15), $h_0 = H(u) = u/\sqrt{1+u^2}$, $h_1 = H'(u) = 1/[1+u^2]^{3/2}$ with $u = w\mu + \mu_I$. Equations (13)-(15) express responses of $\mu(t)$, $\gamma(t)$ and $S(t)$ to correlated inputs with $\mu_I(t)$, $\gamma_I(t)$ and $S_I(t)$.

Stationary properties

A stationary solution of Eqs. (13)-(15) yields

$$\mu = H(w\mu + \mu_I)/(\lambda - \alpha^2/2), \quad \textbf{(16)}$$

$$= (w\mu + \mu_I)/(\lambda - \alpha^2/2), \quad (\text{for } w\mu + \mu_I = r_m) \quad \textbf{(17)}$$

$$= r_m/(\lambda - \alpha^2/2), \quad (\text{for } w\mu + \mu_I \ ? \ r_m) \quad \textbf{(18)}$$

$$\gamma = \frac{[\gamma_I + \alpha^2\mu^2 + \beta^2 + (2h_1 wN\rho/Z)]}{2(\lambda - \alpha^2 + h_1 w/Z)}, \quad \textbf{(19)}$$

$$\rho = \frac{[\gamma_I(1+ZS_I) + \alpha^2\mu^2 + \beta^2]}{2N(\lambda - \alpha^2 - h_1 w)}. \quad \textbf{(20)}$$

Equations (12), (19) and (20) yield the synchronization ratio S given by

$$S = \frac{Z\gamma_I S_I(\lambda - \alpha^2) + h_1 w(\gamma_I + \alpha^2\mu^2 + \beta^2)}{(\gamma_I + \alpha^2\mu^2 + \beta^2)[Z(\lambda - \alpha^2) - h_1 w(Z-1)] + h_1 wZ\gamma_I S_I}, \quad \textbf{(21)}$$

$$= \frac{\gamma_I S_I}{(\gamma_I + \alpha^2\mu^2 + \beta^2)}, \quad (\text{for } w = 0) \quad \textbf{(22)}$$

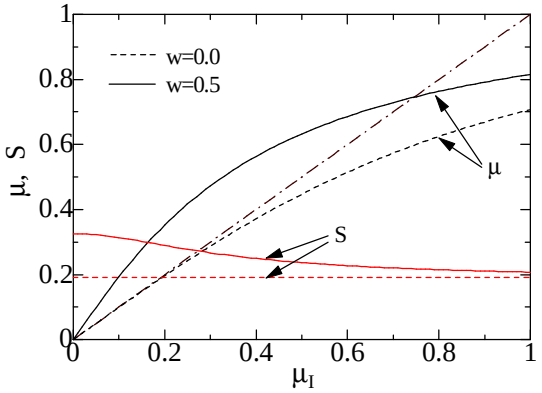

Figure 1. (Color online) Stationary values of μ and S as a function of μ_I for $w = 0.0$ (dashed curves) and $w = 0.5$ (solid curves) with $\gamma_I = 0.2$ and $S_I = 0.2$ ($\lambda = 1.0$, $\alpha = 0.0$, $\beta = 0.1$, and $N = 100$), the chain curve expresses $\mu = \mu_I$.

$$= \frac{h_1 w}{[Z(\lambda - \alpha^2) - (Z-1)h_1 w]}. \quad (\text{for } S_I = 0) \quad \textbf{(23)}$$

Figures 1 shows the μ_I dependences of μ and S for $w = 0.0$ (dashed curves) and $w = 0.5$ (solid curves) with $\gamma_I = 0.2$, $S_I = 0.2$. We note that for $w = 0$, μ is increased with increasing μ_I after the gain function of $H(u)$, while S is independent of μ_I. In contrast, for finite w, μ is much increased than that for $w = 0$. The chain line expresses $\mu = \mu_I$.

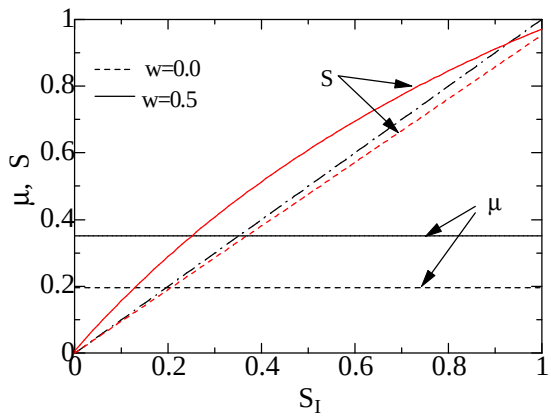

Figure 2. (Color online) Stationary values of μ and S as a function of S_I for $w = 0.0$ (dashed curves) and $w = 0.5$ (solid curves) with $\mu_I = 0.2$ and $\gamma_I = 0.2$ ($\lambda = 1.0$, $\alpha = 0.0$, $\beta = 0.1$, and $N = 100$), the chain curve expressing $S = S_I$.

Figure 2 shows the S_I dependences of μ and S for $w=0.0$ (dashed curves) and $w=0.5$ (solid curves) with $\mu_I=0.2$ and $\gamma_I=0.1$. S is increased with increasing S_I as expected. For $w=0$, μ is independent of S_I, as Eqs. (16)-(18) show. For $w=0.5$, S is much increased compared to that for $w=0.0$.

It is necessary to note that the μ_I dependence of μ is modified by multiplicative noise (α). Figure 3 shows the $\mu_I-\mu$ relation for various α values. With increasing α, μ shows a steeper increase for larger α because of the $(\lambda-\alpha^2/2)$ factor in Eq. (16). The recent experiment of prefrontal cortex showing that the $f-I$ curve has the increased sensitivity at large I with increasing input fluctuation (Arsiero et al., 2007). This is interpreted as due to a shorten, effective refractory period by fluctuation, which is shown by a calculation using the IF model (Arsiero et al., 2007).

The dependence of S on S_I is plotted in Fig. 4 for various values of ensemble size N ($\lambda=1.0$, $\alpha=0.5$, $\beta=0.2$, $w=0.5$). It is shown that the synchrony S is more increased in smaller system. The result for $N=100$ is nearly the same as that for $N=\infty$.

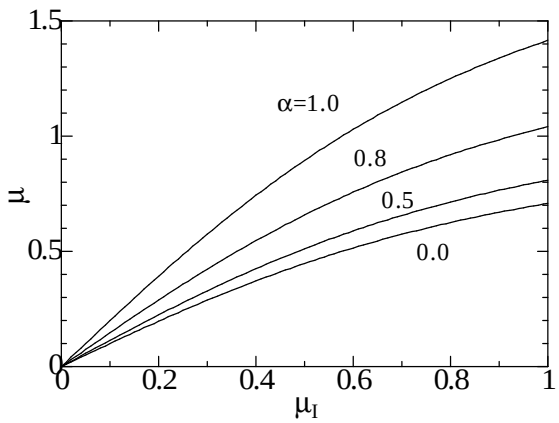

Figure 3. μ as a function of μ_I for various α values with $\lambda=1.0$ and $w=0.0$.

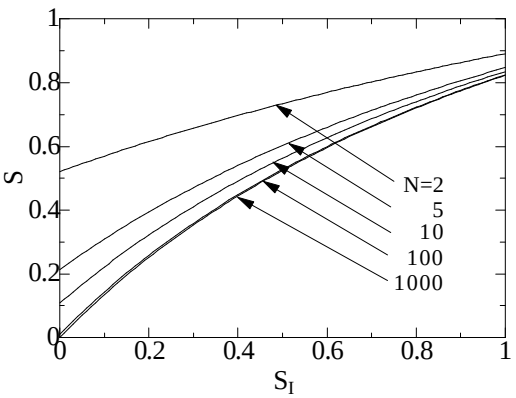

Figure 4. S as a function of S_I for various N with $\mu_I=0.2$, $\gamma_I=0.2$, $\lambda=1.0$, $\alpha=0.5$, $\beta=0.2$ and $w=0.5$.

Dynamical properties

In order to study the dynamical properties of the neuronal ensemble given by Eqs. (1)-(3), we have performed direct simulations (DSs) by using the Heun method with a time step of 0.0001: DS results are averages of 100 trials otherwise noticed. AMM calculations have been performed for Eqs. (13)-(15) by using the fourth-order Runge-Kutta method with a time step of 0.01. We consider an ensemble with $w=0.5$ and $N=100$ as a typical example. Calculated responses to mean-, fluctuation- and synchrony-driven pulse inputs are shown in Figs. 5, 6 and 7, where solid and dashed curves show results of the AMM and DS, respectively.

A. Mean-driven inputs

First we apply a mean-driven pulse input given by

$$\mu_I(t)=0.4\,\Theta(t-40)\Theta(60-t)+0.1, \qquad \textbf{(24)}$$

with $\gamma_I(t)=0.1$ and $S_I(t)=0.1$, where $\Theta(x)$ expresses the Heaviside function: $\Theta(x)=1$ for $x>0$ and zero otherwise.

Figures 6(a)-(d) show $\mu(t)$, $\gamma(t)$, $S(t)$ and $C_v(t)$ where the variability $C_v(t)$ is defined by

$$C_v(t)=\sqrt{\gamma(t)}/\mu(t). \qquad \textbf{(25)}$$

Chain curves in Figs. 5(a), (b) and (c) express input signals of $\mu_I(t)$, $\gamma_I(t)$ and $S_I(t)$, respectively. An increase in an applied mean-driven input at $40\le t<60$ induces an

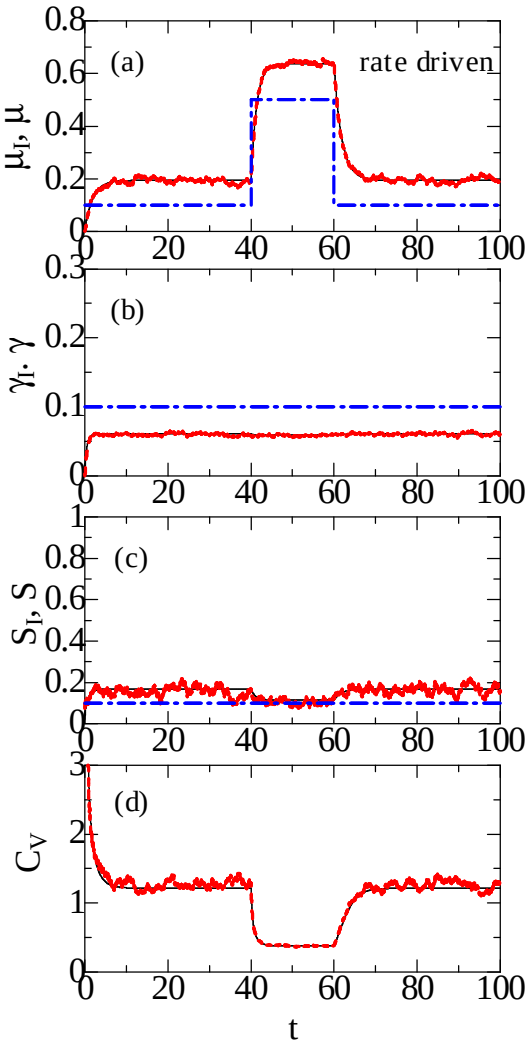

Figure 5. (Color online) The time courses of $\mu(t)$, $\gamma(t)$, $S(t)$ and $C_v(t)$ for mean-driven pulse input given by Eq. (24) with $\gamma_I = 0.1$ and $S_I = 0.1$. Solid and dotted curves express results of the AMM and DS, respectively: chain curves express inputs of $\mu_I(t)$, $\gamma_I(t)$ and $S_I(t)$ ($\lambda = 1.0$, $\alpha = 0.1$, $\beta = 0.1$, $w = 0.5$ and $N = 100$).

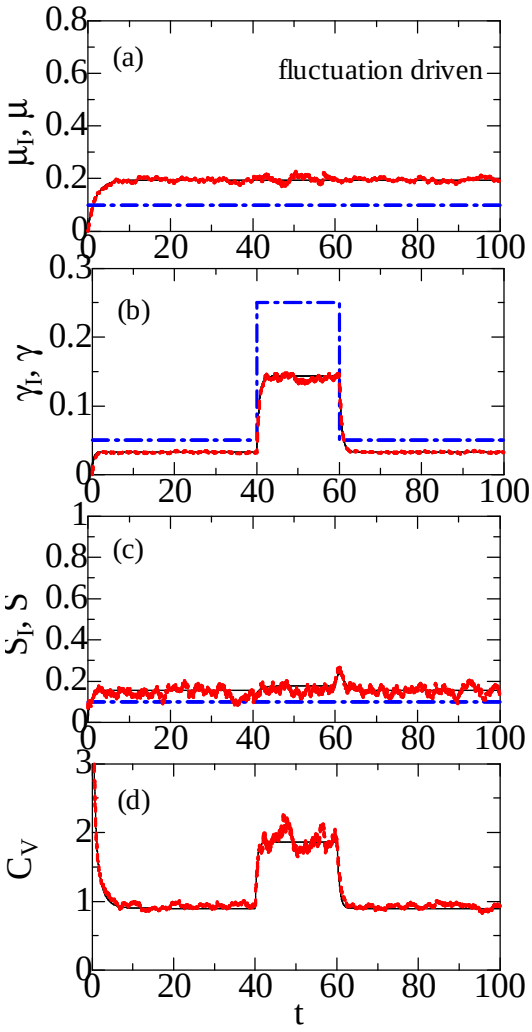

Figure 6. (Color online) The time courses of $\mu(t)$, $\gamma(t)$, $S(t)$ and $C_v(t)$ for fluctuation-driven pulse input given by Eq. (26) with $\mu_I = 0.1$ and $S_I = 0.1$. Solid and dotted curves express results of the AMM and DS, respectively: chain curves express inputs of $\mu_I(t)$, $\gamma_I(t)$ and $S_I(t)$ ($\lambda = 1.0$, $\lambda = 1.0$, $\alpha = 0.1$, $\beta = 0.1$, $w = 0.5$ and $N = 100$).

increase in $\mu(t)$ and decreases in $\gamma(t)$ and $S(t)$ which arise from $\alpha^2\mu^2$ term in Eqs. (13)-(15). By an applied pulse input, $C_v(t)$ is decreased because of the increased μ. The results of the AMM are in good agreement with those of DS.

B. Fluctuation-driven inputs

Next we apply a fluctuation-driven pulse input:

$$\gamma_I(t) = 0.2\,\Theta(t-40)\Theta(60-t) + 0.05, \qquad \textbf{(26)}$$

with $\mu_I(t) = 0.1$ and $S_I(t) = 0.1$, which are plotted by chain curves in Fig. 6(b). When the magnitude of $\gamma_I(t)$ is increased at $40 \le t < 60$, $\gamma(t)$ and $C_v(t)$ are much increased, while there is no changes in $\mu(t)$. $S(t)$ is modified only at t : 40 and t : 60, where the input pulse is on and off.

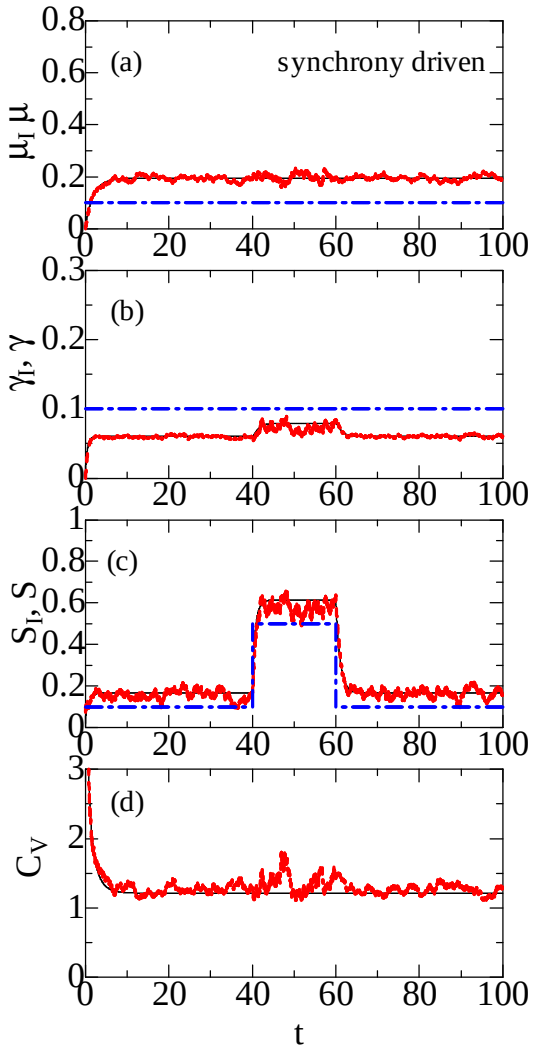

Figure 7. (Color online) The time courses of $\mu(t)$, $\gamma(t)$, $S(t)$ and $C_v(t)$ for synchrony-driven pulse input given by Eq. (27) with $\mu_I = 0.1$ and $\gamma_I = 0.1$. Solid and dotted curves express results of the AMM and DS, respectively: chain curves express inputs of $\mu_I(t)$, $\gamma_I(t)$ and $S_I(t)$ ($\lambda = 1.0$, $\alpha = 0.1$, $\beta = 0.1$, $w = 0.5$ and $N = 100$).

C. Synchrony-driven inputs

We apply a synchrony-driven pulse input:

$$S_I(t) = 0.4\,\Theta(t-40)\Theta(60-t) + 0.1, \qquad \textbf{(27)}$$

with $\mu_I(t) = 0.1$ and $\gamma_I(t) = 0.1$, which are plotted by chain curves in Fig. 7(c). An increase in synchrony-driven input at $40 \le t < 60$ induces increases in $S(t)$, $\gamma(t)$ and $C_v(t)$, but no changes in $\mu(t)$. This is because $\mu(t)$ is decoupled from the rest of variables in Eqs. (13)-(15).

3. Discussion

Independent component analysis

It is interesting to estimate multivariate input signals from multiple output signals. Such a procedure has been provided in various methods such as Bayesian estimation and independent component analysis (ICA) (Hyvärinen et al., 2001). Here we consider ICA, which was originally developed for a linear mixing system, and then it has been extended to linear and nonlinear dynamical systems. ICA has revealed many interesting applications in various fields such as biological signals and image processing. A vector $\mathbf{x}$ of output signals is a real function $\mathbf{F}$ of a vector $\mathbf{s}$ of input sources:

$$\mathbf{x} = \mathbf{F}(\mathbf{s}). \qquad \textbf{(28)}$$

The dimension of $\mathbf{s}$ is assumed to be the same or smaller than that of $\mathbf{x}$. If components of $\mathbf{s}$ are statistically independent and if only one of the source signals is allowed to have a Gaussian distribution, ICA may extract a vector $\mathbf{y}$ with a function $\mathbf{G}$ given by

$$\mathbf{y} = \mathbf{G}(\mathbf{x}), \qquad \textbf{(29)}$$

from which we may estimate the original source as $\mathbf{s}$ **;** $\mathbf{y}$ (Hyvärinen et al., 2001).

A. Coexistence of mean- and synchrony-driven inputs

First we will discuss the case when mean- and synchrony-driven inputs are simultaneously applied to the model. We consider the mean-driven sinusoidal input and synchrony-driven toothsaw input, given by

$$\mu_I(t) = 0.1[1 - \cos(2\pi t / 20)] + 0.1, \qquad \textbf{(30)}$$

$$S_I(t) = 0.01\,\mathrm{mod}(t, 50), \qquad \textbf{(31)}$$

with $\gamma_I(t) = 0.1$ where $\mathrm{mod}(a,b)$ denotes the mod function expressing the residue of a divided by b. Two panels in Fig. 8(a) show $\mu_I(t)$ and $S_I(t)$, and those in Fig. 8(b) show $\mu(t)$ and $S(t)$ calculated by the AMM. We note a little distortion in $S(t)$ due to a cross talk from $\mu(t)$. Assuming $\mathbf{s} = (\mu_I, S_I)^{\dagger}$ and $\mathbf{x} = (\mu, S)^{\dagger}$, we have made an analysis of our result by using ICA. Two panels in Fig. 8(c)

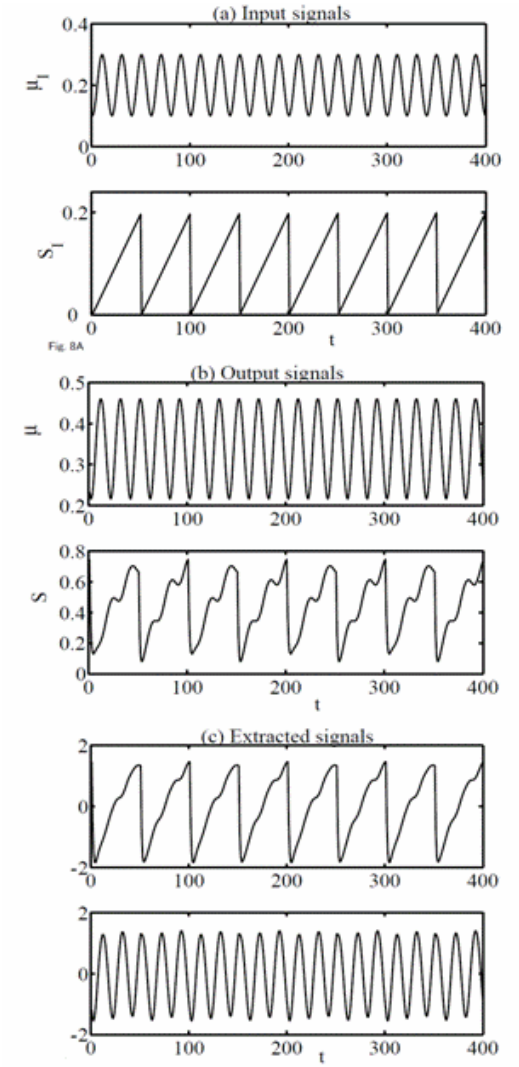

Figure 8. ICA separation of the AMM result for mean- and synchrony-driven inputs: (a) source input signals: (b) output signals: (c) extracted signals by fast ICA ($\lambda = 1.0$, $\alpha = 0.1$, $\beta = 0.1$, $w = 0.5$ and $N = 100$) (see text).

show two components of y extracted from $\mathrm{x} = (\mu, S)^{\dagger}$ shown in Fig. 8(a) with the use of the fast ICA program.

Although the ICA program is designed for linear, mixing signals, we have employed it for our qualitative discussion. We note that results shown in Fig. 8(c) fairly well reproduce the original, sinusoidal and toothsaw signals in Fig. 8(a).

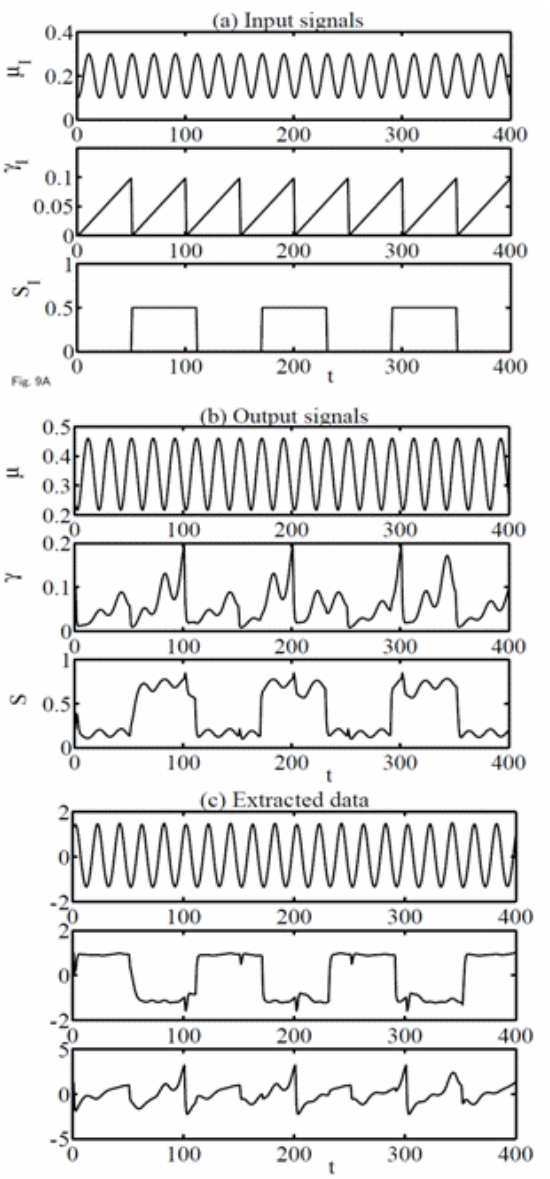

Figure 9. ICA separation of the AMM result for mean-, fluctuation and synchrony-driven inputs: (a) source input signals; (b) output signals: (c) extracted signals by fast ICA ($\lambda = 1.0$, $\alpha = 0.1$, $\beta = 0.1$, $u_{Ii} = N_E^{-1} \sum_j w_{IE}\, r_{Ej} - (N_I - 1)^{-1} \sum_{k(\neq i)} w_{II}\, r_{Ik} + I_{Ii}.$ and $N = 100$) (see text).

B. Coexistence of mean-, fluctuation- and synchrony-driven inputs

Next we consider the case where three kinds of inputs are simultaneously applied. They are mean-driven sinusoidal signal, fluctuation-driven toothsaw signal and synchrony-driven square pulse signal, given by

$$\mu_I(t) = 0.1[1 - \cos(2\pi t / 20)] + 0.1, \qquad \textbf{(32)}$$

$$\gamma_I(t) = 0.002 \,\mathrm{mod}(t, 50), \quad \textbf{(33)}$$

$$S_I(t) = 0.5\,\Theta(-\cos(2\pi t / 120)). \quad \textbf{(34)}$$

Three panels in Fig. 9(a) show the input signals of $\mu_I(t)$, $\gamma_I(t)$ and $S_I(t)$. Output signals of $\mu(t)$, $\gamma(t)$ and $S(t)$ calculated in the AMM are shown in three panels of Fig. 9(b). $\gamma(t)$ and $S(t)$ are a little distorted by a cross talk. We have made an analysis of our result by using ICA, assuming $\mathrm{s} = (\mu_I, \gamma_I, S_I)^\dagger$ and $\mathrm{x} = (\mu, \gamma, S)^\dagger$. Three panels of Fig. 9(c) show signals extracted by the fast ICA. Extracted sinusoidal and square signals are similar to those of input signals, though the fidelity of a toothsaw signal is not satisfactory. This is partly due to the fact that the fast ICA program adopted in our analysis is developed for linear mixing models, but not for dynamical nonlinear models.

These ICA analyses shown Figs. 8 and 9 suggest that the mean rate, fluctuation and synchrony may independently carry information in our population rate-code model.

A comparison with previous studies

Various attempts have been proposed to obtain the firing-rate model, starting from spiking neuron models (Amit and Tsodyks, 1991; Ermentrout, 1994; Shriki et al, 2003; Aviel and Gerstner 2006; Oizumi et al., 2007). It is difficult to analytically calculate the firing rate based on the firing model, except for the IF-type model (Burkitt, 2006a, 2006b). In the coupled IF model, the dynamics of the membrane voltage $v_i(t)$ of the neuron i ($=1-N$) is given by

$$\frac{dv_i}{dt} = -\frac{v_i}{\tau_m} + I_i(t), \quad \textbf{(35)}$$

where τ_m denotes the relaxation time of the membrane and $I_i(t)$ stands for an input to neuron i. When the mean-field and diffusion approximations are adopted, the input signal is given by

$$I_i(t) = J\mu_I(t) + \beta(t)\xi_i(t), \quad \textbf{(36)}$$

where $\beta(t) = \sqrt{J\gamma_I(t)}$, J is the all-to-all coupling, $\mu_I(t)$ and $\gamma_I(t)$ denote the mean and fluctuation, respectively, of input signals, and $\xi_i(t)$ expresses zero-mean Gaussian white noise with correlations given by $<\xi_i(t)\,\xi_j(t')>=\delta_{ij}\,\delta(t-t')$. The firing of neuron is assumed to occur at $t = t_f$ when the voltage $v(t)$ crosses the threshold $S_E = 0.08$ from below, and then the voltage is reset to the potential v_r: $v(t_f) = \theta$, and $v(t_f + 0) = v_r$. The firing rate $r(t)$ is expressed by

$$r(t) = \frac{\beta(t)^2}{2}\left[-\frac{\partial p(v,t)}{\partial v}\right]_{v=\theta}, \quad \textbf{(37)}$$

where the probability distribution $p(v,t)$ is calculated by the FPE with the boundary conditions at $v = \theta$ and $S_E(t)$ and the normalization condition. For the stationary state, we get

$$\frac{1}{r} = \tau_r + \left(\frac{2}{\beta^2}\right)\int_{v_r}^{\theta} du\, e^{\lambda_m (u - I/\lambda_m)^2/\beta^2} \times \int_{-\infty}^{u} dv\, e^{-\lambda_m (v - I/\lambda_m)^2/\beta^2}, \quad \textbf{(38)}$$

where $t = 50$, $\lambda_m = 1/\tau_m$ and τ_r stands for the refractory period. In order to discuss the dynamics of firing rate, it is necessary to solve the FPE to get $p(v,t)$ by numerical methods (Lindner and Schimanski 2001). Equation (37) shows that if information of input signal is encoded in fluctuation of $\gamma_I(t)$, its transmission is instantaneous, as experimentally observed (Lindner and Schimanski 2001; Silbergberg et al., 2004).

By adopting the IF model, Renart et al. (2007) have heuristically derived effective equations of motion for the average firing rate μ_V and variance σ_V^2 of the interspike interval (ISI) given by

$$\frac{d\mu_V}{dt} = -\frac{1}{\tau_m}\mu_V + \mu_s, \quad \textbf{(39)}$$

$$\frac{d\sigma_V^2}{dt} = -\frac{2}{\tau_m}\sigma_V^2 + \sigma_s^2, \quad \textbf{(40)}$$

where μ_s and σ_s are determined from the stationary solution obtained from the FPE of the IF model [as given by Eq. (38)]. We note that Eqs. (39) and (40) are equivalent to Eqs. (13) and (14). Our AMM equations given by Eqs. (13)-(15) provides us with not only

equations of motion for mean and fluctuation but also that for synchrony.

Calculations with the use of the IF model have yielded the following results:
(1) increased input firing rate deceases output variability (Renart et al., 07),
(2) increased firing rate decreases synchrony (Brunel, 2000; Burkitt and Clark 2001; Heinzle, König and Salazar, 2007),
(3) increased fluctuation raises firing rate (Arsiero et al., 2007; Lindner et al. 2003),
(4) increased synchrony increases firing rates (Shadlen and Newsome 1998; Salinas and Sejnowski 2001; Burkitt and Calrk 2001; Moreno et al. 2002; Tiesinga and Sejnowski 2004), and
(5) increased synchrony increases variability (Salinas and Sejnowski 2000).

The items (1), (2) and (5) are consistent with our result shown in Figs. 6 and 7. In contrast, items (3) and (4) seem to inconsistent with our result showing that $\mu(t)$ is independent of $\gamma_I(t)$ and $S_I(t)$, as given by Eqs. (13). A number of neuronal experiments have reported little systematic changes in firing rates while the synchronization within an area is modulated (Salinas and Sejnowski, 2001). In particular, the synchrony may be modified without a change in firing rate in some experiments (Riehle et al, 1997; Fries et al., 2001; Grammont and Riehle, 2003). It has been pointed out that such phenomenon may be accounted for by a mechanism of a rapid activation of a few selected interneurons (Tiesinga and Sejnowski, 2004). Recently the absence of a change in firing rate is shown to be explained if the ratio of excitatory to inhibitory synaptic weights of long-range couplings is kept constant in neuron ensembles described by the IF model (Heinzle, König and Salazar, 2007).

Multiple neuron clusters

In many areas of brain, neurons are organized into groups of cells such as columns in the visual cortex. It is interesting to apply the present approach to Wilson-Cowan type multiple clusters with excitatory and inhibitory synapses described by (Wilson and Cowan, 1972)

$$\frac{dr_{Ei}}{dt} = -\lambda_E\, r_{Ei} + H(u_{Ei}) + \alpha_E\, r_{Ei}\, \eta_{Ei}(t) + \beta_E\, \xi_{Ei}(t), \quad \textbf{(41)}$$

$$\frac{dr_{Ii}}{dt} = -\lambda_I\, r_{Ii} + H(u_{Ii}) + \alpha_I\, r_{Ii}\, \eta_{Ii}(t) + \beta_I\, \xi_{Ii}(t), \quad \textbf{(42)}$$

with

$$u_{Ei} = (N_E - 1)^{-1} \sum_{j(\neq i)} w_{EE}\, r_{Ej} - N_I^{-1} \sum_k w_{EI}\, r_{Ik} + I_{Ei}, \quad \textbf{(43)}$$

$$u_{Ii} = N_E^{-1} \sum_j w_{IE}\, r_{Ej} - (N_I - 1)^{-1} \sum_{k(\neq i)} w_{II}\, r_{Ik} + I_{Ii}. \quad \textbf{(44)}$$

Here λ_m stands for the relaxation rate of a neuron in a cluster m ($=E,I$): N_m expresses the number of neurons of a cluster m: α_m and β_m denote the magnitudes of multiplicative and additive noise, respectively, of a cluster m expressed by zero-mean $\eta_{mi}(t)$ and $\xi_{mi}(t)$: w_{mn} is the couplings between neurons in clusters m and n ($w_{EE}>0$, $w_{IE}>0$, $-w_{EI}<0$ and $-w_{II}<0$). By extending the approach presented in this paper, we may obtain AMM equations for averages, fluctuations of local and global variables relevant to excitatory and inhibitory clusters (Hasegawa, 2007b).

Figure 10 shows an example of the calculated synchrony ratios of $S_E(t)$ and $S_I(t)$ in excitatory and inhibitory clusters, respectively, with various sets of couplings when we apply inputs given by

$$I_{mi}(t) = A_m \Theta(t-40)\Theta(50-t) + A_{mb}, \quad (m = E,I) \quad \textbf{(45)}$$

where $A_E = 0.5$, $A_{Eb} = 0.1$, $A_I = 0.3$ and $A_{Ib} = 0.05$: $w1001$, for example, expresses $(w_{EE}, w_{EI}, w_{IE}, w_{EE}) = (1.0, 0.0, 0.0, 1.0)$ (Hasegawa, 2007b). First we discuss the synchrony ratio at the period of $t<40$ and $t>60$ where the pulse input is not relevant. When only the intra-cluster couplings of $w_{EE} = w_{II} = 1.0$ are introduced ($w1001$), we get $S_E = 0.15$ and $S_I = -0.67$, as shown by dashed curve in Fig. 10(b). When only inter-cluster coupling of

$w_{EI}=1.0$ is included ($w0100$), the synchrony in the excitatory cluster is decreased to $S_E=0.08$ (dotted curves in Fig. 10(a). In contrast, when only inter-cluster of $w_{IE}=1.0$ is introduced ($w0010$), the synchrony in the inhibitory cluster is increased to $S_I=0.06$, as shown by dotted curve in Fig. 10(b). When inter-cluster couplings of $w_{EI}=w_{IE}=1.0$ are included ($w0110$), the synchrony ratios almost vanish (chain curves). Solid curves show that when all intra- and inter-cluster couplings are included ($w1111$), we get $S_E=0.24$ and $S_I=0.04$. Next we consider responses to pulses applied at $40\le t<50$, for which the synchrony ratios show rather complicated behavior. When an input pulse is applied at $t=40$, the synchrony ratios are generally decreased while $S_E(t)$ with $w0110$ is increased: $S_E(t)$ with $w0100$ is once decreased and then increased. When an applied pulse disappears at $t=50$, the synchrony ratios are increased in the refractory period though the synchrony ratios for $w0100$ and $w0110$ are decreased. Thus firings of the excitatory-inhibitory cluster show much variety depending on a set of the couplings. Detailed calculation is under consideration and will be reported elsewhere.

4. Conclusion

We have studied responses of neuronal ensembles to three kinds of inputs: mean-, fluctuation- and synchrony-driven inputs, applying DSs and the AMM to the generalized rate-code model (Hasegawa 2007a; 2007b). The ICA of our results has suggested that mean rate, fluctuation and synchrony may carry independent information. It would be interesting to examine this possibility by neuronal experiments using *in vivo* or *in vitro* neuron ensembles.

One of advantages of our rate-code model given by Eqs. (1)-(3) is that we can easily discuss various properties of neuronal ensembles. We hope that our rate-code model shares advantages with phenomenological neuronal models such as teh Wilson-Cowan (Wilson and Cowan, 1972) and Hopfield models (Hopfield, 1984).

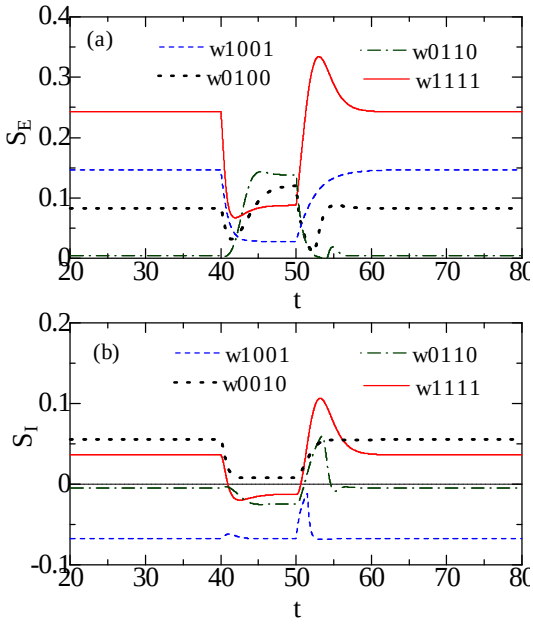

Figure 10. (Color online) Time courses of synchrony ratios of (a) $s_E(t)$ in an excitatory cluster and (b) $s_I(t)$ in an inhibitory cluster for pulse inputs given by Eq. (45) with $A_E=0.5$, $A_{Eb}=0.1$, $A_I=0.3$ and $A_{Ib}=0.05$, $\alpha_E=\alpha_I=0.5$, $\beta_E=\beta_I=0.1$, $N_E=N_I=10$): $w1001$, for example, stands for $(w_{EE},w_{EI},w_{IE},w_{II})=(1.0,0.0,0.0,1.0)$.

It is well known that the Tsallis and Fisher entropies are very important quantities expressing information measures in non-extensive systems (Hasegawa, 2008). Calculations of information entropies are indispensable in deeper understanding of neuronal ensembles with correlated variability. The plasticity of synapses (depression and facilitation) plays important roles in the activity of neurons. Indeed, a memory in brain is accounted for by the plasticity of synapses in the Hopfied model (Hopfield, 1984). A variety of activity in prefrontal cortex in response to sensory stimuli is expected to be explained by dynamic synapses. It is interesting to take into account dynamic synapses in our approach with the rate-code model. These subjects are left for our future study.

5. Materials and Methods

AMM equations for μ, γ and ρ

The Fokker-Planck equation (FPE) for the Langevin equation given by Eq. (1) in the Stratonovich representation is given by

$$\frac{\partial}{\partial t}p=\sum_i\frac{\partial}{\partial r_i}\left[\lambda r_i-H(u_i)\right]p +\frac{\alpha^2}{2}\sum_i\frac{\partial}{\partial r_i}r_i\frac{\partial}{\partial r_i}(r_i\,p) +\frac{\beta^2}{2}\sum_i\frac{\partial^2}{\partial r_i^2}p, \quad \textbf{(46)}$$

where $p=p(\{r_i\},t)$. By using the FPE, we get equations of motion for $\langle r_i\rangle$ and $\langle r_i r_j\rangle$ (Hasegawa, 2006). Expanding r_i around μ as $r_i=\mu+\delta r_i$, and retaining up to their second orders, we have obtained equations of motion for mean and fluctuations in local and global variables, defined by Eqs. (9)-(11) (Hasegawa, 2006). After some manipulations, we get

$$\frac{d\mu}{dt}=-\lambda\mu+h_0+\alpha^2\mu/2, \quad \textbf{(47)}$$

$$\frac{d\gamma}{dt}=-2\lambda\gamma+(2h_1w/Z)(N\rho-\gamma) +2\alpha^2\gamma+\gamma_I+\alpha^2\mu^2+\beta^2, \quad \textbf{(48)}$$

$$\frac{d\rho}{dt}=-2\lambda\rho+2h_1w\rho+2\alpha^2\rho +N^{-1}[\gamma_I(1+ZS_I)+\alpha^2\mu^2+\beta^2], \quad \textbf{(49)}$$

where

$h_0=H(u)=u/\sqrt{1+u^2}$,

$h_1=H'(u)=1/[1+u^2]^{3/2}$,

with $u=w\mu+\mu_I$.

Synchronization ratio

In order to quantitatively discuss the rate synchronization, we first consider the quantity $Q(t)$ given by

$$Q(t)=N^{-2}\sum_{ij}\left\langle[r_i(t)-r_j(t)]^2\right\rangle=2[\gamma(t)-\rho(t)], \quad \textbf{(50)}$$

where $\gamma(t)$ and $\rho(t)$ are given by Eqs. (10) and (11), respectively. When all neurons are firing with the same rate (the completely synchronous state), we get $r_i(t)=R(t)$ for all i, and then $Q(t)=0$ in Eq. (50). On the contrary, in the asynchronous state, we get $Q(t)=2(1-1/N)\gamma(t)\equiv Q_0(t)$ because $\rho=\gamma/N$ (Hasegawa, 2003a; 2007). We may define the normalized ratio for the synchrony of firing rates given by (Hasegawa, 2003a)

$$S(t)=1-Q(t)/Q_0(t)=(N/Z)\left[\rho(t)/\gamma(t)-1/N\right], \quad \textbf{(51)}$$

which is 0 and 1 for complete asynchronous and synchronous states, respectively. Because $S(t)$ is expressed by $\gamma(t)$ and $\rho(t)$ in Eq. (51), it is possible to express the AMM equations in terms of $\mu(t)$, $\gamma(t)$ and $S(t)$, as given by Eqs. (13)-(15).

Relevance to experimental data

Data obtained by neuronal experiments have been analyzed by using various methods .

It is worthwhile to discuss the relevance of experimentally observed data to $\mu(t)$, $\gamma(t)$ and $S(t)$ which are introduced in our study.

Let $x^i{}_k(t)$ be a binned data defined by

$$x_i^{\,k}(t)=1, \quad if\ t_{in}^{\,k}\in[t-\Delta t/2,t+\Delta t/2] \\ =0, \quad otherwise \quad \textbf{(52)}$$

where $t_{in}^{\,k}(t)$ stands for the n th firing time of neuron i of a given k th trial and Δt the width of time window. The firing rate of the neuron i averaged over M trials is given by

$$r_i(t)=(M\Delta t)^{-1}\sum_{k=1}^{M}x_i^{\,k}(t). \quad \textbf{(53)}$$

One conventionally calculates the correlation averaged over time given by

$$C_{ij}(\tau)=\int_{-\infty}^{\infty}\Gamma_{ij}(t,t+\tau)\,dt, \quad \textbf{(54)}$$

with

$$\Gamma_{ij}(t,t')=[r_i(t)-\mu(t)][r_j(t')-\mu(t')], \quad \textbf{(55)}$$

where $\mu(t)$ denotes the average of firing rates given by

$$\mu(t)=N^{-1}\sum_{i=1}^{N}r_i(t). \quad \textbf{(56)}$$

However, $C_{ij}(\tau)$ is not so useful for a study of the response to time-dependent inputs as in our case. The equal-time, auto-and mutual-correlations averaged over an ensemble are given by

$$A(t)=N^{-1}\sum_{i=1}^{N}\Gamma_{ii}(t,t), \quad \textbf{(57)}$$

$$M(t)=[N(N-1)]^{-1}\sum_{i=1}^{N}\sum_{j(\neq i)}^{N}\Gamma_{ij}(t,t). \quad \textbf{(58)}$$

Comparing Eqs. (10) and (12) with Eqs. (57) and (58), we get

$$\gamma(t) = A(t), \quad \textbf{(59)}$$

$$S(t) = M(t) / A(t). \quad \textbf{(60)}$$

Equations (60) shows that $S(t)$ is nothing but the mutual-correlation normalized by the auto-correlation.

Acknowledgements
This work is partly supported by a Grant-in-Aid for Scientific Research from the Japanese Ministry of Education, Culture, Sports, Science and Technology.

References

Anderson RA, Musallam S, Pesaran B. Selecting the signals from a brain-machine interface. Curr Opinion Neurobiol 2004;14:720-726.

Arsiero M, Lüscher H-R, Lndstrom BN. and M. Giugliano, The impact of input fluctuations on the frequency-current relationships of layer 5 pyramidal neurons in the rat medial prefrontal cortex. J Neurosci 2007;27:3274-3284.

Amit DJ, Tsodyks MV. Quantitative study of attractor neural networks retrieving at low spike rates: Substrate-spikes, rates and neuronal gain. Network 1991;2: 259-273.

Aviel Y, Gerstner W. From spiking neurons to rate models: A cascade model as an approximation to spiking neuron models with refractories. Phys Rev E 2006;73:051908.

Burkitt AN. A review of the integrate-and-fire neuron model: I. Homogeneous synaptic input. Bio Cyber 2006a;95:1-19.

Burkitt AN. A review of the integrate-and-fire neuron model: II. Inhomogeneous synaptic input and network properties. Bio Cyber 2006b;95:97-112.

Burkitt AN, Clark GM. Synchronization of the neural response to noisy periodic synaptic input. Neural Comput 2001;13:2639-2672.

Brunel N. Dynamics of sparsely connected networks of excitatory and inhibitory spiking neurons. J Comput Neurosci 2000;8:183-208.

Calvin W, Stevens C. Synaptic noise and other sources of randomness in motoneuron interspike intervals. J Neurophys 1968;31;574-587.

Chance FS, Abbott LF, Reyes AD. Gain modulation from background synaptic input. Neuron 2002;35:773-782.

Chapin JK, Moxon KA, Markowitz RS, Nicolelis MAL. Real-time control of a robot arm using simultaneously recorded neurons in the motor cortex. Nat Neurosci 1999;2:664-670.

de Charms RC, Zador A. Neural representation and the cortical code. Ann Rev Neurosci 2000;23:613-647.

de Oliveira SC, Thiele A, Hoffman KP. Synchronization of neuronal activity during stimulus expectation in a direction discrimination task. J Neurosci 1997;17: 9248-9260.

Eggert J, van Hemmen JL. Unifying framework for neuronal assembly dynamics. Phys Rev E 2000;61:1855-1874.

Ermentrout B. Reduction of conductance-based models with slow synapses to neural nets. Neural Comput 1994;6:679-695.

Feng J, Brown D. Spike output jitter, mean firing time and coefficient of variation. J Phys A 1998;5:239-1252.

Fenton AA, Muller RU. Place cell discharge is extremely variable during individual passes of the rat through the firing field. Proc Natl Acad Sci USA 1998;95:3182-3187.

Fries P, Reynolds JH, Rorie AE, Desimine R. Modulation of oscillatory neuronal synchronization by selective visual attention. Science 2001;291:1560-1563.

Golomb D, Hansel D. The number of synaptic inputs and the synchrony of large, sparse neuronal networks. Neural Comput 2000;12:1095-1139.

Grammont F, Riehle A. Spike synchronization and firing rate in a population of motor cortical neurons in relation to movement direction and reaction time. Biol Cybern 2003;88:360-373.

Hansel D, Mato G. Asynchronous states and the emergence of synchrony in large networks of interacting excitatory and inhibitory neurons. Neural Comput 2003;15: 1-56.

Harris KD. Neural signatures of cell assembly organization. Nat Rev Neurosci 2005;6: 399-406.

Hasegawa H. Responses of a Hodgkin-Huxley neuron to various types of spike-train inputs. Phys Rev E 2000;61:718-726.

Hasegawa H. Dynamical mean-field theory of spiking neuron ensembles: Response to a single spike with independent noise. Phys Rev E 2003a;67:041903.

Hasegawa H. Dynamical mean-field theory of noisy spiking neuron ensembles: Application to Hidgkin-Huxley model. Phys Rev E 2003b;68:041909.

Hasegawa H. Dynaical mean-field approximation to small-world networks of spiking neurons: From local to global and/or from regular to random couplings. Phys Rev E 2004;70:066107.

Hasegawa H. Synchronization in small-world networks of spiking neurons: Diffusive and sigmoid couplings. Phys Rev E 2005;72:056139.

Hasegawa H. N-dependent multiplicative-noise contributions in finite N-unit Langevin models: Augmented moment approach. J Phys Soc Jpn 2006;72:056139.

Hasegawa H. Generalized rate-code model for neuron ensembles with finite populations. Phys Rev E 2007a;75:051904.

Hasegawa H. A generalized rate model for neuronal ensembles. In: M. L. Weiss, editor. Neural network research horizon. Nova Science Publishers, New York; 2007b;61-97.

Hasegawa H. Stationary and dynamical properties of information entropies in nonextensive systems. Phys Rev E 2008;77(in press) [arXiv:0711.3923].

Haskell E, Nykamp DQ, Tranchina D. Population density methods for large-scale modeling of neuronal networks with realistic synaptic kinetics: Cutting the dimension down to size. Network 2000;12:141-174.

Heinzle J, König P, Salazar R. Modulation of synchrony without changes in firing rates. Cogn Neurodyn 2007;1:225-235.

Hyvärinen A, Karhunen J, Oja E. Independent Component Analysis. J. Willey. 2001.

Hopfield JJ. Neural networks and physical systems with emergent collective computational abilities. Proc Natl Acad Sci (USA) 1982;79:2554-2558.

Knight BW. Dynamics of encoding in neuron populations: Some general mathematical features. Neural Comput 2000;12:473-518.

König P, Engel AK, Singer W. Relation between oscillatory activity and long-range synchronization in cat visual cortex. Proc Nat Acad Sci;1995:290-294.

Lindner B, Longtin A, Bulsara A. Analytic expressions for rate and CV of a type I neuron driven by white Gaussian noise. Neural Comput 2003;15:1761-1788.

Lindner B, Schimansky-Geier L. Transmission of noise coded versus additive signals through a neuronal ensembles. Phys Rev Lett 2001;86:2934-2937.

Maldonado PE, Friedman-Hill S, Gray CM. Dynamics of striate cortical activity in the alert macaque: II. Fast time scale synchronization. Cereb Cortex 2000;10: 1117-1131.

Moreno R, de la Rocha J, Renart A, Parga N. Response of spiking neurons to (temporary) correlated inputs. Phys Rev Lett 2002;89:288101.

Oizumi M, Miyawaki Y, Okada M. Higher order effects on rate reduction for networks of Hodgkin Huxley neurons. J Phys Soc Jpn 2007;76:044803.

Omurtag A, Knight BW, Sirovich L. On the simulation of large populations of neurons. J Comput Neurosci 2000;8:51-63.

Pfeuty B, Mato G, Golomb D, Hansel D. The combined effects of inhibitory and electrical synapses in synchrony. Neural Comput 2005;17:633-670.

Renart A, Moreno-Bose R, Wang X-J, Parga N. Mean-driven and fluctuation-driven persistent activity in recurrent networks. Neural Comput 2007;19:1-46.

Reyes AD. Synchrony-dependent propagation of firing rate in iteratively constructed networks in vitro. Nat Neurosci 2003;6:593-599.

Riehle A, Grün S, Diesmann M. and A. Aertsen, Spike synchronization and rate modulation differently involved in motor cortical function. Science 1997;278: 1950-1953.

Rieke F, Warland D, Steveninck R and Bialek W. Spikes-Exploring the neural code. MIT Press; Cambridge; 1996.

Rodriguez R, Tuckwell HC. Statistical properties of stochastic nonlinear dynamical models of single spiking neurons and neural networks. Phys Rev E 1996;54: 5585-5590.

Salinas E, Sejnowski TJ. Correlated neuronal activity and the flow of neural information. Nat Rev Neurosci 2001;2:539-550.

Shadlen MN, Newsome WT. The variable discharge of cortical neurons: Implications for connectivity, computation, and information coding. J Neurosci 1998;18: 3870-3896.

Shriki O, Hansel D, Sompolinsky H. Rate models for conductance-based cortical neuronal networks. Neural Comput 2003;15:1809-1841.

Silberberg G, Bethge M, Markram H, Pawelzik K, Tsodyks M. Dynamics of population rate codes in ensembles of neocortical neurons. J Neurophysiol 2004; 91:704-709.

Softky WR. Simple codes versus efficient codes. Curr Opin Neurobiol 1995;5:239-247.

Softky WR, Koch C. The highly irregular firing of cortical cells is inconsistent with temporal integration of random EPSPs. J Neurosci 1993;13:334-350.

Steinmetz PN, Roy A, Fitzgerald PJ, Hsiao SS, Johnson KO, Niebur E. Attention modulates synchronized neuronal firing in primate somatosensory cortex. Nature 2000;404:187-190.

Tiesinga PHE, José JV, Sejnowski TJ. Comparison of current-driven and conductance-driven neocortical model neurons with Hodgkin-Huxley voltage-gated channel. Phys Rev E 2000 62:8413-8419.

Tiesinga PHE, Sejnowski TJ. Rapid temporal modulation of synchrony by competition in cortical interneuron networks. Neural Comput 2004;16:251-275.

Traub RD, Whittington MA, Stanford IM, Jefferys JG. A mechanism for generation of long-range synchronous fast oscillations in the cortex. Nature 1996;383:621-624.

Tripyer TW, Miller KD. Dynamics of membrane excitability determine inter-spike interval variability: A link between spike generation mechanisms and cortical spike train statistics. Neural Comput 1998;10:1047-1065.

Usher M, Stemmer M, Koch C, Olami Z. Network amplification of local fluctuations causes high spike rate variability, fractal firing patterns and oscillatory local field potentials. Neural Comput 1994;6:795-836.

Ursey WM and Reid RC. Synchronous activity in the visual system. Annu Rev Physiol 1999;61:435-456.

Vaadia E, Haalman I, Abeles M, Bergman H, Prut Y, Slovin H, Aertsen A. Dynamics of neuronal interactions in monkey cortex in relation to behavioral events. Nature 1995;373:515-518.

Wang XJ, Buzsaki G. Gamma oscillation by synaptic inhibition in a hippocampal interneuronal network model. J Neurosci 1996;16:6402-6413.

Wang S, Wang W, Liu F. Propagation of firing rate in a feed-forward neuronal networks. Phys Rev Lett 2006;96:018103.

Wilson HR, Cowan JD. Excitatory and inhibitory interactions in localized populations of model neurons. Biophys J 1972;12:1-24.